frontiers | Frontiers in Energy Research

TYPE Original Research
PUBLISHED 09 April 2024
DOI 10.3389/fenrg.2024.1382444

OPEN ACCESS

EDITED BY
Yan Peng,
China University of Petroleum, Beijing, China

REVIEWED BY
Peng Wu,
Dalian University of Technology, China
Shuai Han,
Hong Kong Polytechnic University, Hong Kong SAR, China

*CORRESPONDENCE
Shangxian Yin,
yinshx03@126.com
Zhenxue Dai,
dzx@jlu.edu.cn

RECEIVED 05 February 2024
ACCEPTED 20 March 2024
PUBLISHED 09 April 2024

CITATION
Liu W, Yin S, Thanh HV, Soltanian MR, Yu Q, Lian H, Yang S, Li Y and Dai Z (2024), Experimental study and application of similar materials in thick coal seam mining. *Front. Energy Res.* 12:1382444. doi: 10.3389/fenrg.2024.1382444

Experimental study and application of similar materials in thick coal seam mining

Wei Liu[1], Shangxian Yin[2]*, Hung Vo Thanh[3,4,5], Mohamad Reza Soltanian[6], Qingyang Yu[1], Huiqing Lian[2], Songlin Yang[1], Yarui Li[1] and Zhenxue Dai[1,7]*

[1]College of Construction Engineering, Jilin University, Changchun, China, [2]Hebei State Key Laboratory of Mine Disaster Prevention, North China Institute of Science and Technology, Beijing, China, [3]Laboratory for Computational Mechanics, Institute for Computational Science and Artificial Intelligence, Van Lang University, Ho Chi Minh City, Vietnam, [4]MEU Research Unit, Middle East University, Amman, Jordan, [5]Faculty of Mechanical - Electrical and Computer Engineering, School of Technology, Van Lang University, Ho Chi Minh City, Vietnam, [6]Departments of Geology and Environmental Engineering, University of Cincinnati, Cincinnati, OH, United States, [7]Key Laboratory of Groundwater Resources and Environment, Ministry of Education, Jilin University, Changchun, China

The orthogonal experiments of similar materials were optimized and analyzed in order to accurately simulate the mechanical properties and the fracture evolution law of thick coal seam overlying strata during mining in this study. The experimental results indicated that similar materials using gypsum and calcium carbonate as cementing agents had a wide range of compressive strength (173.80 kPa–425.95 kPa) and were suitable for simulating various rock properties. Adding an appropriate amount of calcium carbonate can improve the brittleness and mechanical properties of similar materials using gypsum as cementing agents. The failure mode of similar materials transitioned from shear to tensile failure with the increase of the mass ratio of aggregate to cementing agents and the mass ratio of calcium carbonate to gypsum. Moreover, the compressive strength of similar materials rapidly decreased with an increase in the mass ratio of aggregate to cementing materials. And the compressive strength showed an increasing trend with the decrease of the mass ratio of calcium carbonate to gypsum. Moisture content had a significant impact on the density of similar materials, other parameters had small impacts. A thick coal seam mining experimental model was designed based on the experimental results of similar materials, which showed that Qianjiaying Mine may experience basic roof collapse when mining reached 58.1 m. The recommended periodic weighting pace for face pressure on the working face was approximately 15.0 m. Appropriate measures are necessary to adopt to prevent disasters after mining to a length of 58.1 m, followed by every 15.0 m of mining.

KEYWORDS

similar materials, orthogonal experiment, coal seam mining, physical experiment, thick coal seam

1 Introduction

Coal mining often induces fractures in the overlying strata, and continuous development of these fractures can lead to secondary disasters such as collapse, dynamic ground pressure, water influx, and gas outbursts (Ma et al., 2021). To understand the evolution of overlying strata fractures during coal seam mining,

commonly utilized methods include theoretical analysis, numerical simulation, physical simulation, and field monitoring (Kusui et al., 2016; Li et al., 2020; Hou et al., 2021; Ye et al., 2021; Yu et al., 2022; Wang et al., 2023). The high costs associated with field monitoring and testing often pose challenges in practical engineering applications (Yu et al., 2017; Liu S. L. et al., 2020; Marsden et al., 2022). Theoretical analysis and numerical simulation methods can analyze stress distribution patterns and failure modes of overlying strata (Wang et al., 2016; Sun, 2017; Zhang et al., 2019; Liu W. T. et al., 2020; Wang and Dai, 2023). However, relying solely on these methods can result in significant deviations from reality due to the complexity of rock mechanics. In contrast, physical simulation involves physical experiments that recreate on-site geological conditions. Through laboratory experiments, this approach provides in-depth insights into the stress conditions, movement processes, and failure modes of overlying strata (Yang et al., 2021; Shang et al., 2023). Many scholars have extensively explored strata movement, surface subsidence, and mining-induced stresses using similar material simulation methods (Shahani, 2005; Meguid et al., 2008; Cheng et al., 2016; Nardean et al., 2021; Liu et al., 2023). In physical experiments, the selection and proportions of raw materials critically influence the accuracy of the experiments (Ye et al., 2014; Shi et al., 2020).

Many researchers explored the selection and proportions of similar materials, the cementing materials of similar materials typically consist of cement, gypsum, or calcium carbonate (Zhuo et al., 2018; Duan et al., 2021; Zhang et al., 2021). Shi et al. (2021) employed aggregates (river sand and mica powder) and cementing agents (lime, gypsum, and cement) to simulate the development of fractures in overlying strata. The study indicated that cement exhibited higher strength than gypsum and effectively bonds with river sand. However, the significant differences in cement strength between actual engineering and similar simulation experiments, coupled with the time-dependent nature of cement hardening and the relatively short duration of simulation experiments, may lead to substantial errors (Zhu et al., 2017; Mendes and Thompson, 2019; Rodrigues and de Souza Mendes, 2019). Additionally, temperature significantly influenced the cement hardening process (Iesaka et al., 2004; Termkhajornkit and Barbarulo, 2012; Wang, 2022). Gypsum serves as a widely employed gas-hardening cementing agent in similar material experiments, possessing lower strength, lower cost, and a faster hardening process, making it potentially more suitable for simulating low-strength and brittle materials (Misnikov, 2018; Lesovik et al., 2020; Shi et al., 2022). However, pure gypsum is suitable for simulating linear elastic materials, the mechanical properties of overlying strata in coal seams often exhibit nonlinearity with significant deformations (Mou et al., 2020). Consequently, employing gypsum alone as a cementing agent in similar materials experiments may not effectively emphasize its residual strength and deformation characteristics (Li and Wang, 2022). To enhance the mechanical performance and deformability of the similar materials, the calcium carbonate was recommended to add as a cementing agent to improve the performance of similar materials (Zhuo et al., 2018; Shi et al., 2020). However, the addition of calcium carbonate can have an impact on the strength and curing time of similar materials.

In order to more accurately simulate the mechanical properties and fracture development patterns for overlying strata of thick coal seams, this study utilizes gypsum and calcium carbonate as cementing agents, river sand as aggregate, and water as a regulator, employing an orthogonal experimental design. Similar material experiments were conducted in order to systematically investigate the mechanical properties of similar materials under different mass ratios of aggregate to cementing agents, mass ratios of calcium carbonate to gypsum, and to explore the influence of moisture content and curing time on the density of similar materials. On the basis of similar materials experiments, a physical experiment was carried out with Qianjiaying coal mine as the engineering background to explore the development law and evolution mechanism of overlying strata fractures during thick coal seam mining, and the collapse law of overlying strata in thick coal seams was studied.

2 Experimental program of similar materials

2.1 Experiment design

An orthogonal experimental design was employed in this study, and gypsum and calcium carbonate were utilized as cementing agents, river sand as aggregate, and water as a regulator. In order to systematically investigate the mechanical properties of similar materials under various parameters, four factors were considered as experimental variables: mass ratio of aggregate to cementing agents, mass ratio of calcium carbonate to gypsum, moisture content, and curing time. Based on the $L_{25}(5^4)$ method, with each factor including five experimental levels, the orthogonal experiment details are presented in Table 1.

In the experiment, the mass ratio of aggregate to cementing agents was divided into five levels (i.e., 4:1, 6:1, 8:1, 10:1, and 12:1). The mass ratio of calcium carbonate to gypsum was set at the following: 8:2, 6:4, 5:5, 4:6, 2:8. Moisture content was set: 7%, 8%, 9%, 10%, and 11%. Curing time was set at 1 day, 3 days, 5 days, 7 days, and 9 days. A total of 25 similar material specimens were prepared, labeled as S1 to S25. The specimen details are listed in Table 2.

2.2 Sample preparation

All specimens were fabricated using river sand, gypsum, calcium carbonate, and water. Initially, measured amounts of river sand, gypsum, and calcium carbonate powders were uniformly mixed. Subsequently, a specific quantity of water was added, and the mixture was thoroughly stirred. The mixed materials were poured into a plastic double-open mold with a diameter of 50 mm and a height of 100 mm. Approximately 25 mm of the mixture was poured for each layer, followed by compaction until the height of specimen reached 100 mm. It is noteworthy that during the pouring of upper layers of the mixture, the interface of the lower layer was scratched to avoid interface effects, the sample production process is depicted in Figure 1. After casting, specimens were cured at room temperature (20°C) according to the curing times in Table 2 and subsequently demolded. To minimize experimental errors, each group of specimens included three identical samples, and the

TABLE 1 Orthogonal experiment details.

Level	Mass ratio of aggregate to cementing agents	Mass ratio of calcium carbonate to gypsum	Moisture content (%)	Curing time (day)
1	4:1	8:2	7	1
2	6:1	6:4	8	3
3	8:1	5:5	9	5
4	10:1	4:6	10	7
5	12:1	2:8	11	9

average of their physical-mechanical parameters was taken as the final result.

2.3 Mechanical testing of similar materials

The weight of the specimens was measured after the curing period. Subsequently, uniaxial compression tests of the specimens were carried out using a universal testing machine, as illustrated in Figure 2. The loading protocol employed displacement control, loading at a rate of 1.0 mm/min. During the loading process, stress results of the specimens were obtained by an automated data acquisition system, and the failure modes of specimens were observed.

3 Experimental results and discussion

3.1 Experimental results

The test results for all specimens are presented in Table 3, and the failure modes are illustrated in Figure 3. The failure modes can be classified into shear failure and tensile failure. Figure 3 depicts the failure modes under different mass ratios of aggregate to cementing agents. When the mass ratio of aggregate to cementing agents was less than 8:1, the specimens exhibited shear failure. As the mass ratio of aggregate to cementing agents increased, the failure mode gradually transitioned to tensile failure. The change of failure modes is attributed to the weakening of the cementing effect between aggregates as the amount of cementing agents decreased, resulting in a shift towards tensile failure, a similar experimental results were observed in reference (Wen et al., 2020).

Figure 4 illustrates the failure modes under various mass ratios of calcium carbonate to gypsum, while keeping the mass ratio of aggregate to cementing agents constant. When the mass ratio of calcium carbonate to gypsum was less than 4:6, the specimens exhibited shear failure. However, as the mass ratio of calcium carbonate to gypsum increased, the failure mode transitioned from shear failure to tensile failure. This is due to the significant improvement in the plasticity of similar materials when calcium carbonate was added to gypsum as a cement. However, gypsum controlled the strength of similar materials. When an appropriate amount of calcium carbonate (i.e., 20%–40% in this study) was added, it significantly enhanced the overall performance of similar materials, resulting in shear failure. However, when the mass ratio of calcium carbonate to gypsum exceeded 4:6, the similar materials failed to achieve the required strength of experimental materials, exhibiting poorer overall performance and, consequently, tensile failure.

Furthermore, the failure mode of similar materials was significantly influenced by curing time, as illustrated in Figure 5. When the curing time was equal to or less than 3 days, the specimens primarily exhibited tensile failure (Figures 5A, B). However, with a curing time of 5 days or longer, shear failure became the predominant failure mode (Figures 5C–E). This can be attributed to insufficient solidification of the cementing agents (i.e., calcium carbonate and gypsum) when the curing time was relatively short, resulting in poor overall integrity and a tendency towards tensile failure. Conversely, if the curing time was 5 days or longer, complete solidification of the cementing materials occurred, leading to better overall integrity and shear failure becoming the main failure mode.

It is worth noting that with curing times of 1 day or 3 days, the increase in the mass ratio of calcium carbonate to gypsum led to a transition from tensile failure to shear failure and subsequently back to tensile failure. Analyzing the case of a 3-day curing time, this transition is primarily because of the addition of calcium carbonate, which shortens the curing time of the cementing agents. This results in similar materials achieving higher strength under shorter curing times, leading to a shift from tensile to shear failure modes (Figures 6A–C). However, as the calcium carbonate content increased and gypsum content decreased, despite the reduced curing time of similar materials, the strength of the similar materials failed to meet the requirements, and the failure mode was tensile failure (Figures 6D, E).

Figure 7 illustrates the failure modes under various moisture content. Specimens exhibited tensile failure at a moisture content of 7% (Figure 7A), while shear failure became the predominant mode with a moisture content of 8% (Figure 7B). However, when the moisture content exceeded 8%, the specimens exhibited tensile failure (Figures 7C–E). This is because at a moisture content of 7%, the moisture was insufficient, and the cementing agents cannot fully function, resulting in lower strength of similar materials and a failure mode characterized by tensile failure. At a moisture content of 8%, comprehensive reactions occurred in the similar materials, establishing a strong bond with the aggregate, leading to higher specimen strength and shear failure. Beyond 8% moisture content, excess moisture negatively impacted material bonding, and excessive hydration reactions in the cementing material reduced specimen strength, resulting in tensile failure.

3.2 Compressive strength

The uniaxial compressive strength of similar materials under various factors is presented in Figure 8 and Table 4. With an increase

10.3389/fenrg.2024.1382444

TABLE 2 Orthogonal test schemes for similar materials.

Specimen ID	Mass ratio of aggregate to cementing agents	Mass ratio of calcium carbonate to gypsum	Moisture content (%)	Curing time (day)	Specimen ID	Mass ratio of aggregate to cementing agents	Mass ratio of calcium carbonate to gypsum	Moisture content (%)	Curing time (day)
S1	4:1	8:2	7	1	S14	8:1	4:6	11	1
S2	4:1	6:4	9	7	S15	8:1	2:8	8	7
S3	4:1	5:5	11	3	S16	10:1	8:2	9	9
S4	4:1	4:6	8	9	S17	10:1	6:4	11	5
S5	4:1	2:8	10	5	S18	10:1	5:5	8	1
S6	6:1	8:2	11	7	S19	10:1	4:6	10	7
S7	6:1	6:4	8	3	S20	10:1	2:8	7	3
S8	6:1	5:5	10	9	S21	12:1	8:2	8	5
S9	6:1	4:6	7	5	S22	12:1	6:4	10	1
S10	6:1	2:8	9	1	S23	12:1	5:5	7	7
S11	8:1	8:2	10	3	S24	12:1	4:6	9	3
S12	8:1	6:4	7	9	S25	12:1	2:8	11	9
S13	8:1	5:5	9	5					

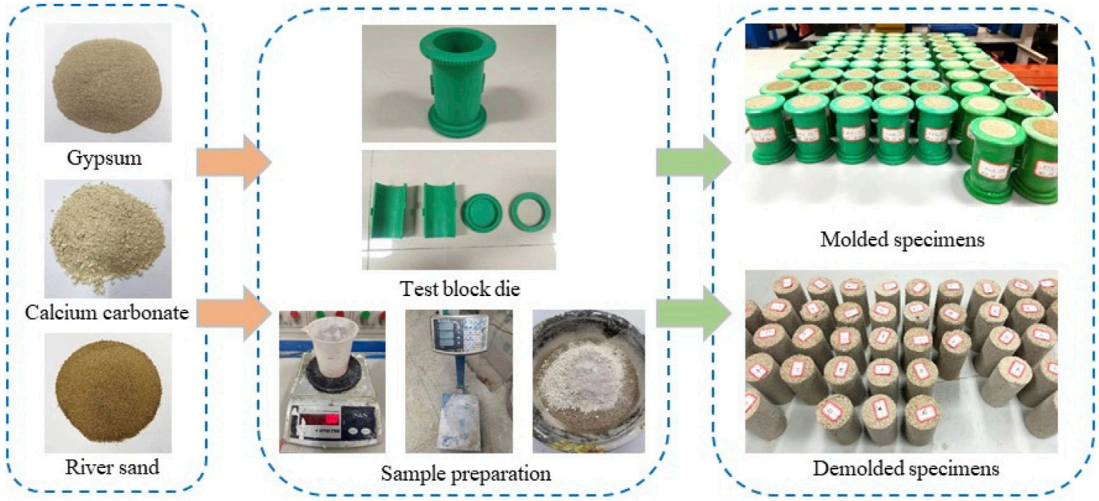

FIGURE 1
Material preparation and sample production process.

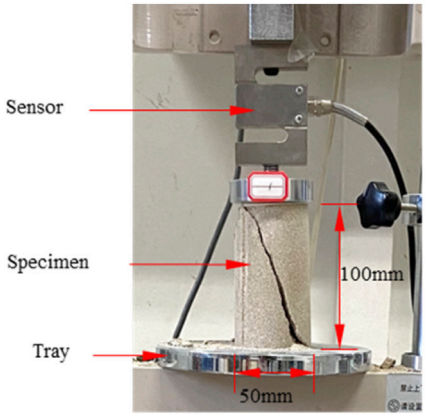

FIGURE 2
Universal testing machine.

in the mass ratio of aggregate to cementing agents, the compressive strength rapidly decreased, which is owing to a higher mass ratio of aggregate to cementing agents resulting in insufficient cementing agent content, leading to weaker bonding between aggregates and a subsequent reduction in compressive strength. When the mass ratio of aggregate to cementing agents was constant, an increase in gypsum content led to an increase trend in the compressive strength of similar materials, which is due to gypsum content determining the strength of similar materials, with calcium carbonate showing no significant enhancement in compressive strength. However, when the gypsum content was excessively high, similar materials exhibited noticeable brittleness, and the addition of calcium carbonate can improve the properties of similar materials (Shen et al., 2023; Sun et al., 2023).

As curing time extended, the compressive strength of specimens initially increased and then stabilized. For samples with a mass ratio of calcium carbonate to gypsum greater than or equal to 5:5, the compressive strength of similar materials stabilized after curing 3 days, while for samples with a lower mass ratio of calcium carbonate to gypsum, the compressive strength stabilized after curing 5 days. This is due to the relatively short hydration time of calcium carbonate, which shortened the curing time of the cementing agents. Moisture content had minimal impact on compressive strength. With an increase in moisture content, the compressive strength initially increased and then reduced, with the highest compressive strength observed at the moisture content of 8%. Table 4 indicates that the mass ratio of aggregate to cementing agents and the mass ratio of calcium carbonate to gypsum had a significant impact on the compressive strength of similar materials, with a range of 252.15 kPa. In contrast, moisture content had a small effect, with a range of only 52.73 kPa.

3.3 Density

The density results of similar materials under different factors are presented in Table 5; Figure 9 illustrates the variation in density under various influencing factors. Moisture content had significant impact on the density of similar materials. When the moisture content exceeded 8%, the density had a rapid increase, rising from 1,746.32 kg/m^3 to 1,860.89 kg/m^3. In comparison, the mass ratio of aggregate to cementing agents, the mass ratio of calcium carbonate to gypsum, and curing time had relatively small effects on density.

From the above analysis, using river sand as aggregate, gypsum and calcium carbonate as cementing agents, and water as a regulator, the compressive strength of the prepared similar materials ranges from 173.80 kPa to 425.95 kPa, indicating a significant variation in compressive strength. This variability allowed for the preparation of similar materials with corresponding strengths, demonstrating a strong adaptability to similar model tests. To obtain the uniaxial compressive strength and density of similar materials using gypsum and calcium carbonate as cementing materials, a multivariate regression analysis was conducted on various experimental parameters. The uniaxial compressive strength (Y_1) and density (Y_2) of the specimens can be expressed by Eqs 1, 2, respectively.

TABLE 3 Orthogonal test results for similar materials.

Specimen ID	Proportion number	Density (kg/m^3)	Uniaxial compressive strength (kPa)	Failure mode	Specimen ID	Proportion number	Density (kg/m^3)	Uniaxial compressive strength (kPa)	Failure mode
S1	4:8:2	1,777.20	247.90	T	S14	8:4:6	1,878.22	177.32	S
S2	4:6:4	1,800.64	534.78	S	S15	8:2:8	1,737.58	442.29	S
S3	4:5:5	1,868.28	413.89	S	S16	10:8:2	1,765.27	107.52	T
S4	4:4:6	1,685.10	453.30	S	S17	10:6:4	1,859.75	210.57	S
S5	4:2:8	1,826.96	479.88	S	S18	10:5:5	1,788.79	122.55	T
S6	6:8:2	1,844.71	301.66	T	S19	10:4:6	1,807.59	203.72	S
S7	6:6:4	1,774.39	452.10	T	S20	10:2:8	1,749.17	433.89	T
S8	6:5:5	1,790.06	318.98	T	S21	12:8:2	1,745.73	78.98	S
S9	6:4:6	1,752.46	434.24	T	S22	12:6:4	1,794.65	98.34	T
S10	6:2:8	1,792.36	269.30	S	S23	12:5:5	1,718.56	145.22	S
S11	8:8:2	1,810.19	205.35	T	S24	12:4:6	1,765.94	148.62	S
S12	8:6:4	1,765.22	308.66	S	S25	12:2:8	1,853.50	397.83	T
S13	8:5:5	1,815.71	405.27	T					

Note: S represents shear failure, and T represents tensile failure.

10.3389/fenrg.2024.1382444

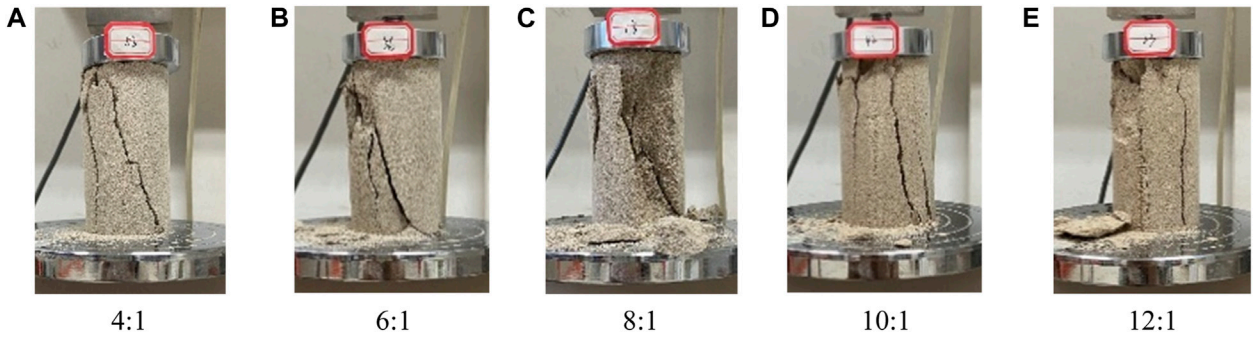

FIGURE 3
Failure modes under various mass ratios of aggregates to cementing agents. **(A)** 4:1 **(B)** 6:1 **(C)** 8:1 **(D)** 10:1 **(E)** 12:1.

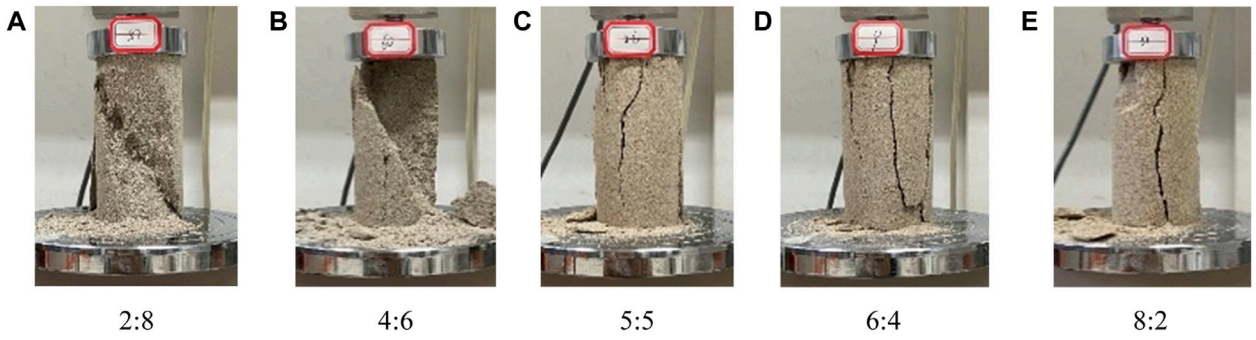

FIGURE 4
Failure modes under various mass ratios of calcium carbonate to gypsum. **(A)** 2:8 **(B)** 4:6 **(C)** 5:5 **(D)** 6:4 **(E)** 8:2.

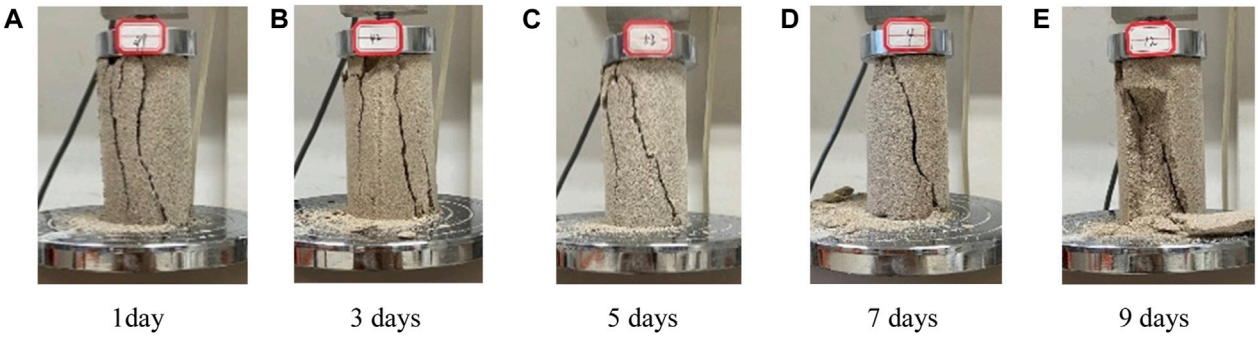

FIGURE 5
Failure modes at different curing times. **(A)** 1 day **(B)** 3 days **(C)** 5 days **(D)** 7 days **(E)** 9 days.

$$Y_1 = 671.746 - 35.369X_1 - 38.342X_2 - 9.344X_3 + 6.795X_4 \quad (1)$$

$$Y_2 = 1573.438 - 1.430X_1 + 0.131X_2 + 27.631X_3 - 4.030X_4 \quad (2)$$

where X_1 is the mass ratio of aggregates to cementing agents, X_2 is the mass ratio of calcium carbonate to gypsum, X_3 is the moisture content, and X_4 is the curing time.

4 Engineering application

The comprehensive mechanized mining face with large mining height in thick coal seams has a large mining space, and the degree and range of disturbance to the overlying strata during mining are high. This will lead to changes in the laws of strata movement, roof

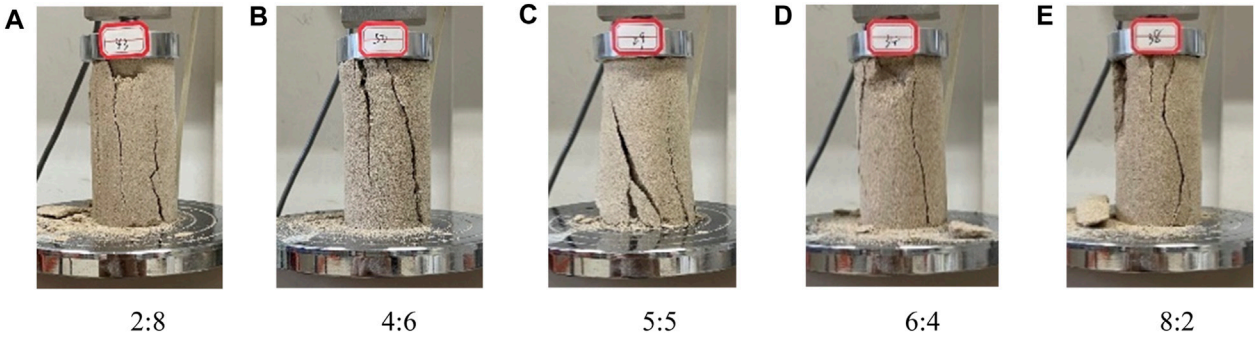

FIGURE 6
Failure modes with different mass ratios of calcium carbonate to gypsum for curing 3 days. **(A)** 2:8 **(B)** 4:6 **(C)** 5:5 **(D)** 6:4 **(E)** 8:2.

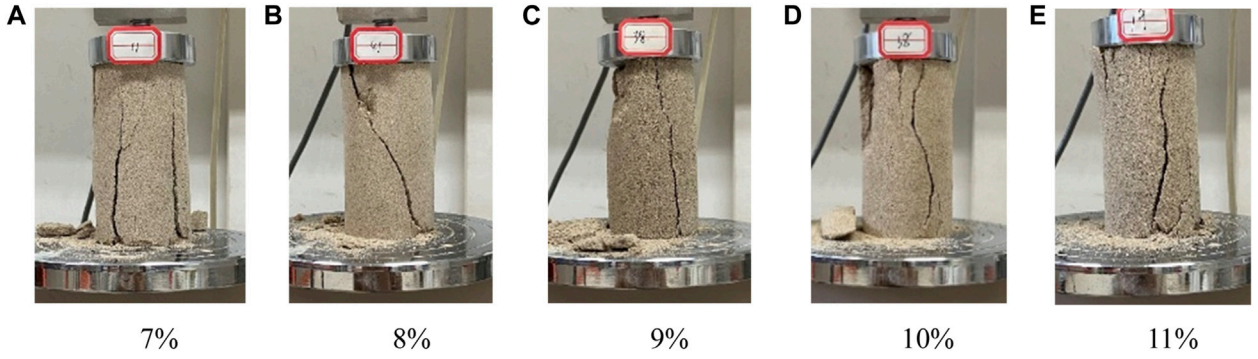

FIGURE 7
Failure modes at different moisture contents. **(A)** 7% **(B)** 8% **(C)** 9% **(D)** 10% **(E)** 11%.

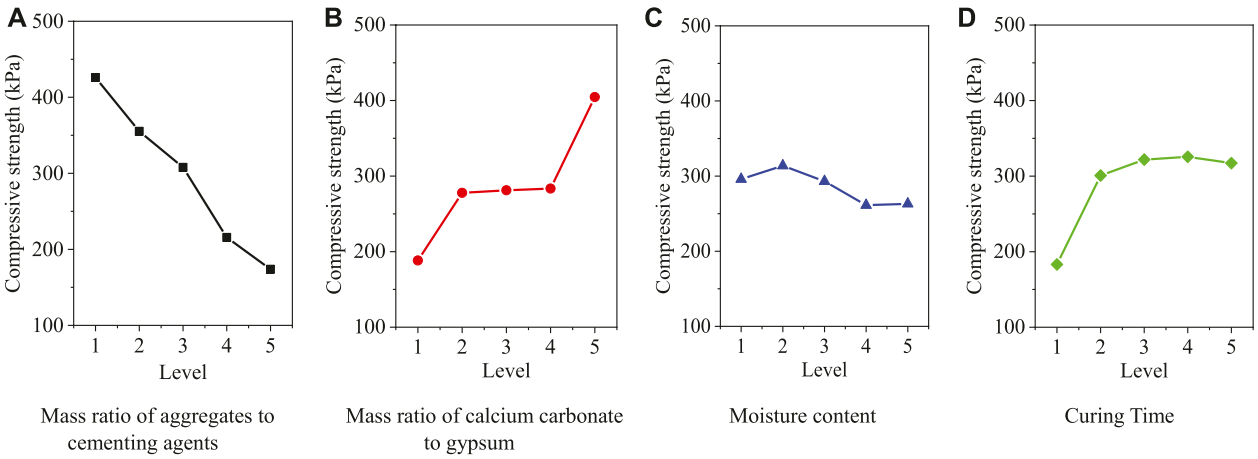

FIGURE 8
Uniaxial compressive strength of similar materials. **(A)** Mass ratio of aggregates to cementing agents **(B)** Mass ratio of calcium carbonate to gypsum **(C)** Moisture content **(D)** Curing Time.

structure morphology, and the development characteristics of overlying strata fractures. Relevant research using physical simulation experiments was conducted to gain a deeper understanding of these features. This study selected the 2078 working face of Qianjiaying Mine as the research object, which is located in Tangshan City, Hebei Province and belongs to the Kailuan Coalfield (Figure 10A). The coal seam in the 2078 mining face of Qianjiaying Mine is well preserved, with a

TABLE 4 Range analysis of compressive strength (kPa).

Factors	Level 1	Level 2	Level 3	Level 4	Level 5	Range
Mass ratio of aggregates to cementing agents	425.95	355.26	307.78	215.65	173.80	252.15
Mass ratio of calcium carbonate to gypsum	188.28	277.82	281.18	283.44	404.64	216.36
Moisture content	295.98	313.84	293.10	261.25	263.14	52.73
Curing time	183.08	300.77	321.79	325.53	317.26	147.69

TABLE 5 Density results (unit: kg/m^3).

Factors	Level 1	Level 2	Level 3	Level 4	Level 5	Range
Mass ratio of aggregates to cementing agents	1,791.64	1,790.80	1,801.38	1,794.11	1,775.68	25.71
Mass ratio of calcium carbonate to gypsum	1,788.62	1,798.93	1,796.28	1,777.86	1,791.91	21.07
Moisture content	1,752.52	1,746.32	1,787.98	1,805.89	1,860.89	114.57
Curing time	1,806.24	1,793.59	1,800.12	1,781.82	1,771.83	34.41

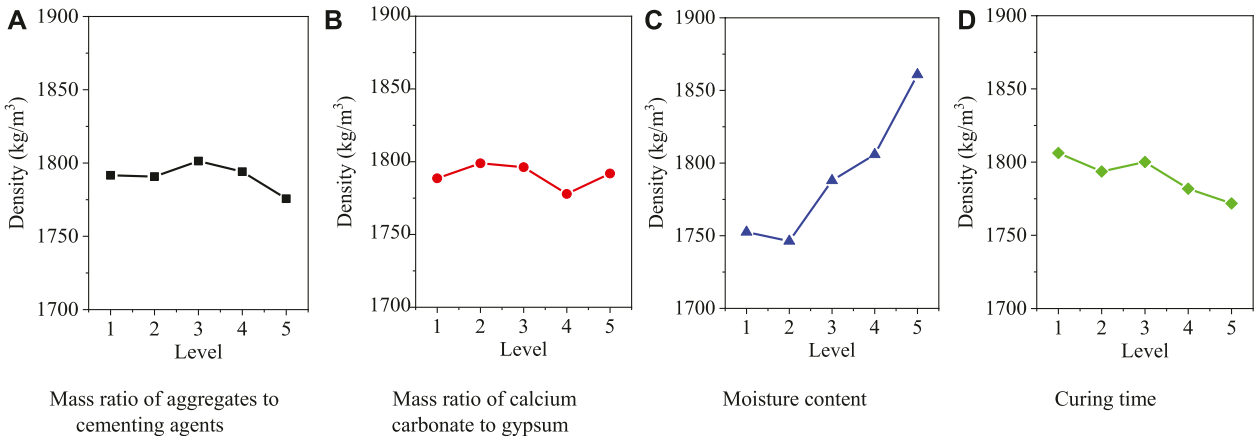

FIGURE 9
Density results under various factors. **(A)** Mass ratio of aggregates to cementing agents **(B)** Mass ratio of calcium carbonate to gypsum **(C)** Moisture content **(D)** Curing time.

thickness of 6.0 m and typical characteristics of thick coal seams. The stratigraphic columns is shown in Figure 10B. The elevation range of the mining face is −719.3 m ~ -781.8 m, and the elevation selected for model testing is −736.4 m. The ground elevation range is +20.9 m~+24.2 m, and the model test takes +24.0 m. The total thickness of the overlying strata is taken as 760.4 m. The working face has a length of 822.0 m and a tilt length of 206.5 m. The dip angle of the coal seam ranges from 3° to 11°, with an average of 7°, and is simulated in a horizontal coal seam manner. The coal mining method was comprehensive mechanized coal mining, with a mining speed of 3.0 m per day.

Based on the geological data of the 2078 working face of Qianjiaying Mine, a geometric similarity ratio of 1:100 was taken for physical simulation experiments based on similarity theory. The overlying strata was mainly composed of fine sandstone, siltstone, medium sandstone, and coarse sandstone, with uniaxial compressive strengths of 30.2 MPa, 33.5 MPa, 36.1 MPa, and 38.9 MPa, respectively, corresponding to a density of 2,382 kg/m^3, 2,632 kg/m^3, 2,330 kg/m^3, and 2,200 kg/m^3. The size of the similar model was set to be 2.0 m (length), 1.354 m (height), and 0.175 m (width). The height of the coal seam mining was set to 6 cm. The proportions for the similar materials were determined based on similarity theory and Eqs 1, 2. The displacement monitoring points in the experimental model were set at the top and bottom of the model, as well as the position of the main key layer (65 cm away from the top of the coal seam), with an interval of 10 cm. The experimental model is shown in Figure 11. The coal seam was mined at a speed of 3.0 cm/2.4 h, while monitoring the dynamic changes in overlying strata displacement and fractures during the thick coal seam mining process. The monitoring equipment and data acquisition system are shown in Figure 12.

A

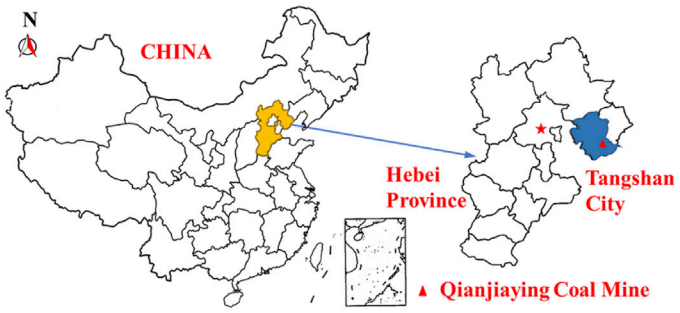

B

Column	Number	Lithology	Thickness (m)	Distance from coal seam roof (m)
	20	Silty sandstone	3.4	122.4
	19	Medium sandstone	12.4	119.0
	18	Fine sandstone	9.8	106.6
	17	Silty sandstone	2.6	96.8
	16	Fine sandstone	2.2	94.2
	15	Silty sandstone	4.6	92.0
	14	Medium sandstone	4.0	87.4
	13	Gritstone	6.8	83.4
	12	Fine sandstone	2.4	76.6
	11	Silty sandstone	16.9	74.2
	10	Fine sandstone	6.0	57.3
	9	Medium sandstone	5.0	51.3
	8	Fine sandstone	6.9	46.3
	7	Medium sandstone	7.2	39.4
	6	Gritstone	4.0	32.2
	5	Fine sandstone	9.8	28.2
	4	Silty sandstone	15.2	18.4
	3	Fine sandstone	3.2	3.2
	2	Coal 7	6.0	6.0
	1	Silty sandstone	10.0	10.0

FIGURE 10
(A) Location map of study area; **(B)** Stratigraphic columns.

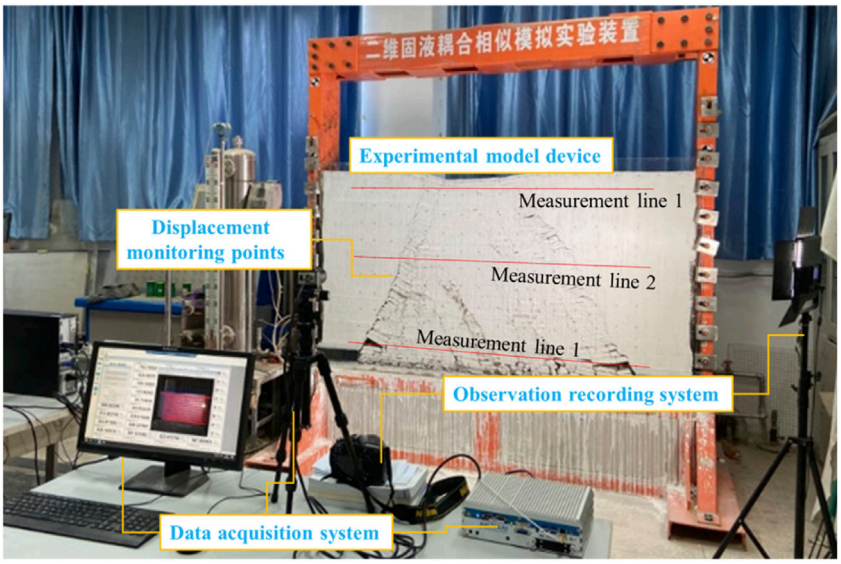

FIGURE 11
Testing system for thick coal seam mining overlying strata.

Evolution process of overlying strata fractures during thick coal seam mining is depicted in Figure 13. It can be observed that with a coal seam extraction of 36.7 cm, the immediate roof collapsed, and fractures started to appear in the overlying strata. This condition persisted until a coal seam extraction length of 52.0 cm, indicating that when the mining distance is relatively short, the coal seam extraction had no significant impact on the overlying strata. After a coal seam extraction length of 58.1 cm, a large-scale collapse occurred in the roof, with a fracture height of 41.5 cm and a separation space height of 4.1 cm. On the pillar side, the overlying strata above the basic roof directly sheared off, forming an articulated structure on the working face side. The initial weighting pace for the first face pressure was 58.1 cm. After a coal seam extraction of 94.9 cm on the working face, the main key layer fractured, and the overlying strata collapsed entirely, resulting in intense face pressure. The fracture angle on the working face side significantly increased (from 64° to 71°). With the expansion of the extraction distance, the extent of fractures development gradually extended in a trapezoidal pattern and tended to stabilize. The fractures exhibited a distinct "two-side fractured zones, middle compacted zone" morphology, and the periodic weighting pace for face pressure on the working face was approximately 15.0 cm.

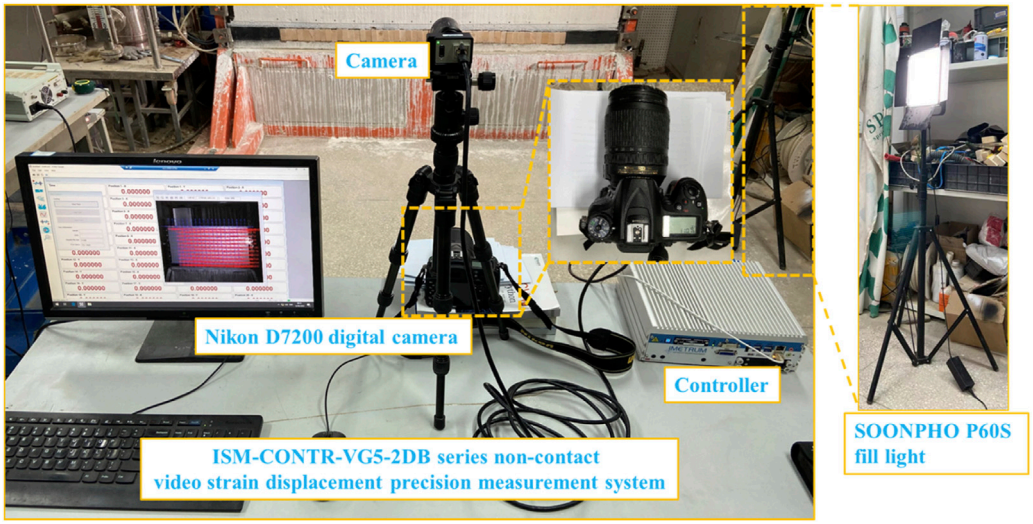

FIGURE 12
ISM-CONTR-VG5-2DB series non-contact video strain and displacement precision measurement system.

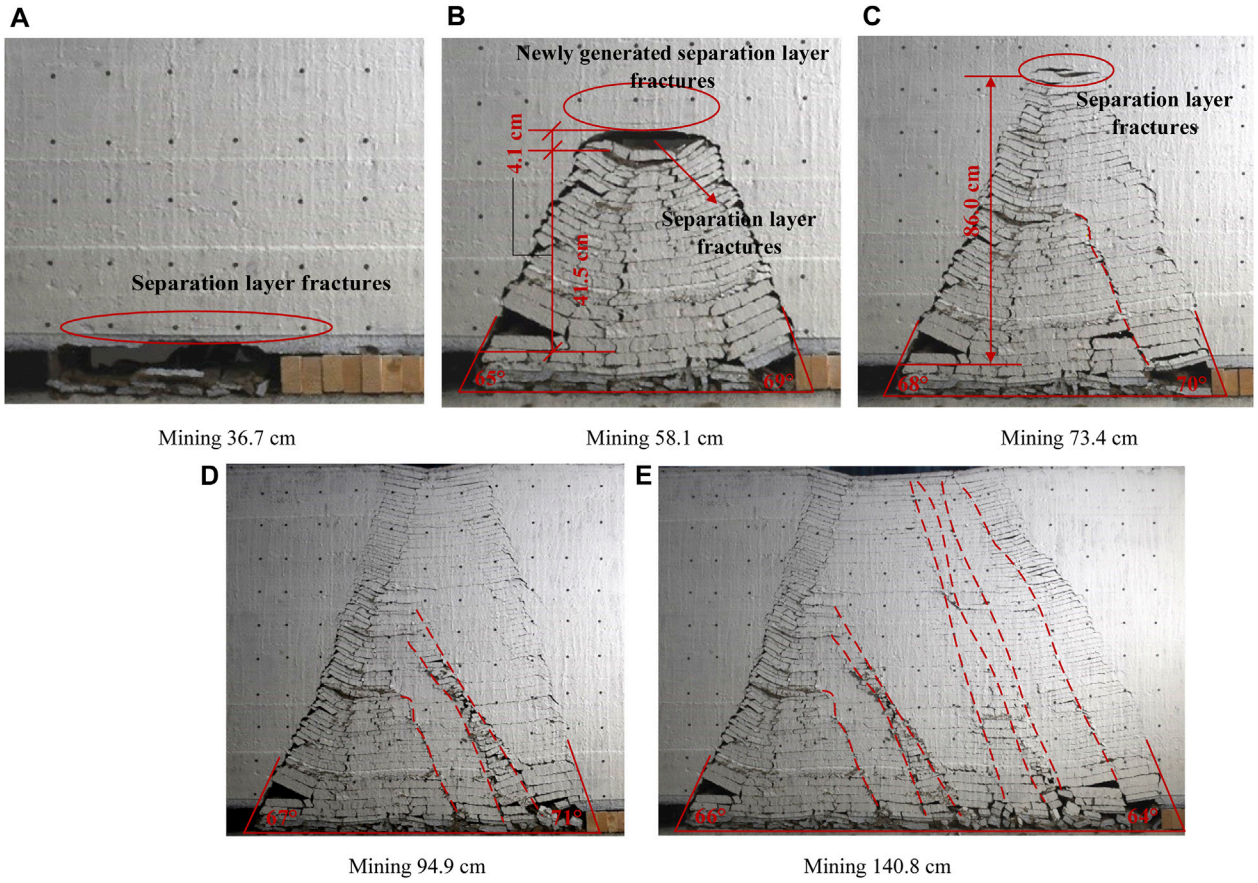

FIGURE 13
Evolution process of overlying strata fractures during thick coal seam mining. **(A)** Mining 36.7 cm **(B)** Mining 58.1 cm **(C)** Mining 73.4 cm **(D)** Mining 94.9 cm **(E)** Mining 140.8 cm.

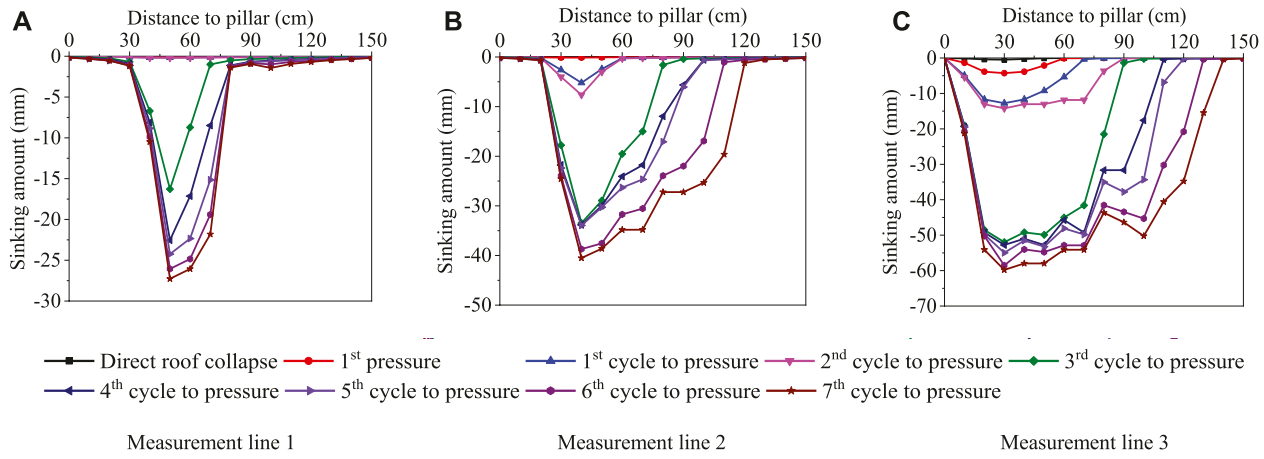

FIGURE 14
Sinking curves of monitoring points at different mining stages. **(A)** Measurement line 1 **(B)** Measurement line 2 **(C)** Measurement line 3.

Continuous monitoring was conducted on the displacement monitoring points during the excavation process of the model, as illustrated in Figure 14. With the decrease in the distance between the overlying strata and the top of the coal seam, the horizontal range of strata settlement gradually expanded. The displacement curve transformed from a "funnel shape" to an "inverted trapezoid." The settlement height of the strata gradually increased, ultimately settling at 27.27 cm, 40.51 cm, and 59.82 cm, respectively. During the third periodic weighting of face pressure, significant displacements were observed in all three displacement monitoring lines, indicating a notable influence of the key layer on overlying strata displacement. The displacement curves of the rear monitoring points on the working face gradually overlapped, and the amount of strata settlement stabilized.

The results of the physical experiment showed that Qianjiaying Mine may experience a basic roof collapse when mining reached 58.1 m. The periodic weighting pace for face pressure on the working face was approximately 15.0 m. It is suggested to adopt appropriate measures to prevent disasters after mining to a length of 58.1 m, followed by every 15.0 m of mining.

5 Conclusion

In order to investigate the mechanical properties of thick coal seams, an orthogonal experiment was conducted using gypsum and calcium carbonate as cementing agents to study the effects of different parameters on the failure modes, compressive strength, and density of similar materials. The main conclusions are as follows:

1. The failure mode of similar materials can be divided into shear and tensile failure, and the specimens exhibited significant shear failure when the mass ratio of aggregate to cementing agents was less than 8:1, and the failure mode transitioned from shear to tensile failure with the increase of the mass ratio of aggregate to cementing agents. Moreover, shear failure was observed when the mass ratio of calcium carbonate to gypsum was below 4:6, but the failure mode transitioned from shear failure to tensile failure with the ratio increased.
2. Shear failure was the predominant failure mode when the curing time was enough. At a moisture content of 8%, the specimens exhibited shear failure, while at moisture contents exceeding 8%, the specimens showed tensile failure.
3. The compressive strength rapidly decreased with an increase in the mass ratio of aggregate to cementing materials. When the mass ratio of aggregate to cementing agents was constant, an increase in gypsum content led to an increase trend in the compressive strength of similar materials. An appropriate increase in calcium carbonate content can shorten the curing time. Moisture content has a minimal impact on compressive strength, with the highest compressive strength observed at the moisture content of 8%.
4. Moisture content had significant impact on the density of similar materials. When the moisture content exceeded 8%, the density had a rapid increase. However, the mass ratio of aggregate to cementing agents, the mass ratio of calcium carbonate to gypsum, and curing time had relatively small effects on density.
5. Based on the model test results, Qianjiaying Mine may experience basic roof collapse when mining reached 58.1 m. The recommended periodic weighting pace for face pressure on the working face was approximately 15.0 m. It is suggested to adopt appropriate measures to prevent disasters after mining to a length of 58.1 m, followed by every 15.0 m of mining.

Data availability statement

The original contributions presented in the study are included in the article/Supplementary material, further inquiries can be directed to the corresponding authors.

Author contributions

WL: Data curation, Investigation, Writing–original draft, Writing–review and editing. SY: Conceptualization, Investigation, Methodology, Writing–review and editing. HT: Writing–review and editing. MS: Writing–review and editing. QY: Conceptualization,

Investigation, Methodology, Writing–review and editing. HL: Investigation, Visualization, Writing–review and editing. SY: Conceptualization, Methodology, Writing–review and editing. YL: Investigation, Visualization, Writing–review and editing. ZD: Conceptualization, Funding acquisition, Investigation, Methodology, Writing–review and editing.

Funding

The author(s) declare financial support was received for the research, authorship, and/or publication of this article. This work is funded by the National Natural Science Foundation of China (Grant numbers: 42141011, U2267217, 42002254, and 51974126).

Acknowledgments

The authors thank Jilin University (JLU) for the support of Program of JLU Science and Technology Innovative Research Team (JLUSTIRT-2019TD-35) and the Engineering Research Center of Geothermal Resources Development Technology and Equipment, Ministry of Education, China.

Conflict of interest

The authors declare that the research was conducted in the absence of any commercial or financial relationships that could be construed as a potential conflict of interest.

Publisher's note

All claims expressed in this article are solely those of the authors and do not necessarily represent those of their affiliated organizations, or those of the publisher, the editors and the reviewers. Any product that may be evaluated in this article, or claim that may be made by its manufacturer, is not guaranteed or endorsed by the publisher.

References

Cheng, W., Sun, L., Wang, G., Du, W., and Qu, H. (2016). Experimental research on coal seam similar material proportion and its application. *Int. J. Min. Sci. Technol.* 26 (5), 913–918. doi:10.1016/j.ijmst.2016.05.034

Duan, H., Zhao, L., and Chen, Y. (2021). Effect of floor failure in fully mechanized caving of extra-thick coal seam in Datong Mining Area. *Arab. J. Geosci.* 14 (11), 1008. doi:10.1007/s12517-021-07436-1

Hou, E., Zhang, M., Sun, X., Jiang, Y., Xie, X., Wang, J., et al. (2021). Study on overburden failure and development height of water conducting fracture zone in shallow coal seam mining. *Coal Eng.* 53 (11), 102–107. doi:10.11799/ce202111020

Iesaka, K., Jaffe, W. L., and Kummer, F. J. (2004). Effects of the initial temperature of acrylic bone cement liquid monomer on the properties of the stem-cement interface and cement polymerization. *J. Biomed. Mater. Res. Part B* 68B (2), 186–190. doi:10.1002/jbm.b.20020

Kusui, A., Villaescusa, E., and Funatsu, T. (2016). Mechanical behaviour of scaled-down unsupported tunnel walls in hard rock under high stress. *Tunn. Undergr. Space Technol.* 60 (1), 30–40. doi:10.1016/j.tust.2016.07.012

Lesovik, V., Drebezgova, M., and Fediuk, R. (2020). Fast-curing composites based on multicomponent gypsum binders. *J. Mater. Civ. Eng.* 32 (9). doi:10.1061/(asce)mt.1943-5533.0003313

Li, R., Chen, L., Ou, Q., Chen, Y., Wang, Y., Ge, R., et al. (2020). Numerical simulation of fractured water-conducting zone by considering native fractures in overlying rocks. *Coal Geol. Explor.* 48 (6), 179–185. doi:10.3969/j.issn.1001-1986.2020.06.024

Li, Z., Wang, X., Hou, Y., and Wu, Z. (2022). Optimization of mechanical properties and water absorption behavior of building gypsum by ternary matrix mixture. *Constr. Build. Mater.* 350, 128910. doi:10.1016/j.conbuildmat.2022.128910

Liu, S. L., Dai, S., Li, W. P., Han, B., He, B., and Luo, J. P. (2020a). A new monitoring method for overlying strata failure height in Neogene laterite caused by underground coal mining. *Eng. Fail. Anal.* 117, 104796. doi:10.1016/j.engfailanal.2020.104796

Liu, W., Dong, S., Yin, S., Dai, Z., Xu, B., Soltanian, M. R., et al. (2023). A new approach for quantitative definition of asymmetrical loading tunnels. *Iran. J. Sci. Technol.-Trans. Civ. Eng.* 47 (1), 457–468. doi:10.1007/s40996-022-00958-y

Liu, W. T., Pang, L. F., Xu, B. C., and Sun, X. (2020b). Study on overburden failure characteristics in deep thick loose seam and thick coal seam mining. *Geomatics Nat. Hazards Risk* 11 (1), 632–653. doi:10.1080/19475705.2020.1737584

Ma, H., Chen, S., Xue, D., Chen, Y., and Chen, Z. (2021). Outlook for the coal industry and new coal production technologies. *Adv. Geo-Energy Res.* 5 (2), 119–120. doi:10.46690/ager.2021.02.01

Marsden, H., Basu, S., Striolo, A., and MacGregor, M. (2022). Advances of nanotechnologies for hydraulic fracturing of coal seam gas reservoirs: potential applications and some limitations in Australia. *Int. J. Coal Sci. Technol.* 9 (2), 27–18. doi:10.1007/s40789-022-00497-x

Meguid, M. A., Saada, O., Nunes, M. A., and Mattar, J. (2008). Physical modeling of tunnels in soft ground: a review. *Tunn. Undergr. Space Technol.* 23 (2), 185–198. doi:10.1016/j.tust.2007.02.003

Mendes, P. R. D., and Thompson, R. L. (2019). Time-dependent yield stress materials. *Curr. Opin. Colloid Interface Sci.* 43, 15–25. doi:10.1016/j.cocis.2019.01.018

Misnikov, O. (2018). The hydrophobic modification of gypsum binder by peat products: physico-chemical and technological basis. *Mire Peat* 21 (1), 1–14. doi:10.19189/MaP.2017.OMB.300

Mou, Y., Zhou, C., Jiang, N., Xiao, W., Du, C., and Meng, X. (2020). Experiment study on proportioning of similar materials in weak surrounding rocks of rich-water faults. *Geotech. Geol. Eng.* 38 (4), 3415–3433. doi:10.1007/s10706-020-01223-7

Nardean, S., Ferronato, M., Zhang, Y., Ye, S., Gong, X., and Teatini, P. (2021). Understanding ground rupture due to groundwater overpumping by a large lab experiment and advanced numerical modeling. *Water Resour. Res.* 57 (3). doi:10.1029/2020wr027553

Rodrigues, E. C., and de Souza Mendes, P. R. (2019). Predicting the time-dependent irreversible rheological behavior of oil well cement slurries. *J. Pet. Sci. Eng.* 178, 805–813. doi:10.1016/j.petrol.2019.03.073

Shahani, A. R. (2005). Some problems in the antiplane shear deformation of bi-material wedges. *Int. J. Solids Struct.* 42 (11-12), 3093–3113. doi:10.1016/j.ijsolstr.2004.11.002

Shang, Y., Zhang, L., Kong, D., Wang, Y., and Cheng, Z. (2023). Overlying strata failure mechanism and gas migration law in close distance outburst coal seams: a case study. *Eng. Fail. Anal.* 148, 107214. doi:10.1016/j.engfailanal.2023.107214

Shen, X., Li, J., Feng, G., Zhao, D., and Liu, Q. (2023). Experimental study on the properties of simulation materials for an aquifuge for a fluid-solid coupling physical similarity model test. *Appl. Sci.-Basel* 13 (15), 8667. doi:10.3390/app13158667

Shi, C., Ma, C., Yang, Y., and Zou, X. (2022). Effects of temperature and humidity on properties of ethylene/vinyl acetate-modified ternary complex mortar. *J. Appl. Polym. Sci.* 139 (19). doi:10.1002/app.52103

Shi, X., Jing, H., Zhao, Z., Gao, Y., Zhang, Y., and Bu, R. (2020). Physical experiment and numerical modeling on the failure mechanism of gob-side entry driven in thick coal seam. *Energies* 13 (20), 5425. doi:10.3390/en13205425

Shi, Y., Ye, Y., Hu, N., Huang, X., and Wang, X. (2021). Experiments on material proportions for similar materials with high similarity ratio and low strength in multilayer shale deposits. *Appl. Sci.-Basel* 11 (20), 9620. doi:10.3390/app11209620

Sun, J. (2017). Mechanics criterion and factors affecting overburden stability in solid dense filling mining. *Int. J. Min. Sci. Technol.* 27 (3), 407–413. doi:10.1016/j.ijmst.2017.03.010

Sun, L., Wang, W., and Xu, J. (2023). Study on proportioning scheme of coal system rocky similar material based on orthogonal test. *Materials* 16 (22), 7113. doi:10.3390/ma16227113

Termkhajornkit, P., and Barbarulo, R. (2012). Modeling the coupled effects of temperature and fineness of Portland cement on the hydration kinetics in cement paste. *Cem. Concr. Res.* 42 (3), 526–538. doi:10.1016/j.cemconres.2011.11.016

Wang, F., Zhang, C., Wei, S., Zhang, X., and Guo, S. (2016). Whole section anchor-grouting reinforcement technology and its application in underground roadways with loose and fractured surrounding rock. *Tunn. Undergr. Space Technol.* 51, 133–143. doi:10.1016/j.tust.2015.10.029

Wang, X. L. (2022). Similar simulation test of overlying rock failure and crack evolution in fully mechanized caving face with compound roof. *Geotech. Geol. Eng.* 40 (1), 73–82. doi:10.1007/s10706-021-01892-y

Wang, Y., Dai, Z., Chen, L., Shen, X., Chen, F., and Soltanian, M. R. (2023). An integrated multi-scale model for CO2 transport and storage in shale reservoirs. *Appl. Energy* 331, 120444. doi:10.1016/j.apenergy.2022.120444

Wang, Y., Dai, Z., Wang, G. S., Chen, L., Xia, Y. Z., and Zhou, Y. H. (2023). A hybrid physics-informed data-driven neural network for CO2 storage in depleted shale reservoirs. *Pet. Sci.* 21, 286–301. doi:10.1016/j.petsci.2023.08.032

Wen, C., Jia, S., Fu, X., Meng, L., and Zhao, Z. (2020). Experimental research and sensitivity analysis of mudstone similar materials based on orthogonal design. *Adv. Mater. Sci. Eng.* 2020, 1–14. doi:10.1155/2020/2031276

Yang, B., Yuan, S., Liang, Y., and Liu, J. (2021). Investigation of overburden failure characteristics due to combined mining; case study, Henan Province, China. *Environ. Earth Sci.* 80 (4), 143. doi:10.1007/s12665-021-09462-4

Ye, D., Liu, G., Gao, F., Xu, R., and Yue, F. (2021). A multi-field coupling model of gas flow in fractured coal seam. *Adv. Geo-Energy Res.* 5 (1), 104–118. doi:10.46690/ager.2021.01.10

Ye, Y., Shi, Y., Wang, Q., Yao, N., Lu, F., and Yue, Z. (2014). Test model research on low strength similar material of Shanghengshan multilayer shale deposit. *Rock Soil Mech.* 35, 114–120. doi:10.16285/j.rsm.2014.s2.033

Yu, B., Zhao, J., and Xiao, H. T. (2017). Case study on overburden fracturing during longwall top coal caving using microseismic monitoring. *Rock Mech. Rock Eng.* 50 (2), 507–511. doi:10.1007/s00603-016-1096-8

Yu, Q., Xu, P., Dai, Z., Yin, S., Soltanian, M. R., and Liu, W. (2022). Numerial analysis of rock joints in tunnel construction during blasting. *Arabian J. Geosci.* 15 (1). doi:10.1007/s12517-021-09304-4

Zhang, Q., Peng, C., Liu, R., Jiang, B., and Lu, M. (2019). Analytical solutions for the mechanical behaviors of a hard roof subjected to any form of front abutment pressures. *Tunn. Undergr. Space Technol.* 85, 128–139. doi:10.1016/j.tust.2018.12.004

Zhang, Z., Zhang, Y., Xu, Y., Zheng, Q., Wang, Z., and Guo, L. (2021). Fracture development and fractal characteristics of overburden rock under repeated mining. *Arab. J. Geosci.* 14 (3), 225. doi:10.1007/s12517-021-06524-6

Zhu, W., Setunge, S., Gamage, N., Gravina, R., and Venkatesan, S. (2017). Evaluating time-dependent reliability and probability of failure of reinforced-concrete bridge components and predicting residual capacity after subsequent rehabilitation. *J. Perform. Constr. Facil.* 31 (3). doi:10.1061/(asce)cf.1943-5509.0000975

Zhuo, H., Qin, B., Shi, Q., and Li, L. (2018). Development law of air leakage fractures in shallow coal seams: a case study in the Shendong Coalfield of China. *Environ. Earth Sci.* 77 (23), 772. doi:10.1007/s12665-018-7961-x